

Article

Association of Rare Earths in Different Phases of Marcellus and Haynesville Shale: Implications on Release and Recovery Strategies

Shailee Bhattacharya, Vikas Agrawal  and Shikha Sharma * 

Department of Geology and Geography, West Virginia University, Morgantown, WV 26506, USA

* Correspondence: shikha.sharma@mail.wvu.edu

Abstract: Hydrocarbon-rich shales have been a major natural gas source in the US over the last decade. These organic-rich shales can also potentially serve as a source of some rare earth elements (REYs). However, the mode of occurrence and the geochemical processes that led to REY enrichment in these shales are still poorly understood. In this study, we investigated the whole-rock REY content and associations of REYs in the different phases of Marcellus and Haynesville Shale samples. A traditional sequential extraction procedure was adopted to understand the association of REYs in (i) exchangeable, (ii) acid-soluble, (iii) pyritic, (iv) organic matter, and (v) silicate fractions. Extraction efficiency was assessed by comparing the mineralogy of the pre- and post-sequential extraction samples using XRD. Elemental ratios such as La/Lu, La/Sm, Gd/Lu, Y/Ho, and Ce and Eu anomalies were utilized to understand whole-rock-normalized REY distribution patterns. Further, the distribution pattern in each extracted phase was examined to account for the relative contribution of phases to REY enrichment. The economic potential of these samples was evaluated by calculating HREE/LREE ratios, outlook coefficients, and by comparing their REY levels with those of coal fly ash deposits. Our results indicate that whole-rock REY content in the analyzed shale samples ranged from 295 to 342 ppm, with Haynesville Shale having a higher concentration than the Marcellus Shale sample. All samples exhibited an MREE–HREE-enriched pattern, indicating that the REY content is primarily contributed by carbonate and siliciclastic inputs. However, the average total REY extraction efficiency was only approximately 20% from the Haynesville samples and 9% from the Marcellus sample. We postulate that the poor REY yield is due to a high amount of refractory aluminosilicate/clay fraction in these samples. We demonstrate that traditional sequential extraction procedures may not be effective for extracting REYs from high organic–high aluminosilicate shale.

Keywords: rare earths; black shale; phase association; sequential extraction

Citation: Bhattacharya, S.; Agrawal, V.; Sharma, S. Association of Rare Earths in Different Phases of Marcellus and Haynesville Shale: Implications on Release and Recovery Strategies. *Minerals* **2022**, *12*, 1120. <https://doi.org/10.3390/min12091120>

Academic Editors: Pei Ni, Mincheng Xu, Tiangang Wang, Junyi Pan and Yitao Cai

Received: 25 July 2022

Accepted: 29 August 2022

Published: 2 September 2022

Publisher's Note: MDPI stays neutral with regard to jurisdictional claims in published maps and institutional affiliations.



Copyright: © 2022 by the authors. Licensee MDPI, Basel, Switzerland. This article is an open access article distributed under the terms and conditions of the Creative Commons Attribution (CC BY) license (<https://creativecommons.org/licenses/by/4.0/>).

1. Introduction

The global drive for green energy has accelerated the need for enhanced mineral resource exploration. As the reliability on clean energy increases, certain rare earth elements, for example, neodymium (Nd), erbium (Er), dysprosium (Dy), yttrium (Y), and terbium (Tb) are considered “critical” as they are at supply risk [1]. This is because the availability of rare earth elements, including Yttrium and Scandium (REY) [2], from conventional ores is decreasing as their demand keeps increasing due to their use in wind energy, solar panels, electrical vehicles, batteries, permanent magnets, ceramics, catalytic converters, etc. [3]. Additionally, there are only a limited number of sources that have significantly contributed to the change in the supply of raw materials [4–10]. It is estimated that the demand for rare earth elements will increase by at least seven times in the next two decades [11]. Traditionally, there are different classification schemes for rare earth elements (REE) in the literature depending on the objectives of the study. Yttrium and Scandium (Y and Sc) are often included in REEs and classified as REYs. However, it is essential to note that

although Y and Sc are grouped together as REYs, they are much lighter than the REEs in the lanthanide series. One of the more popular schemes to understand REY patterns and geochemistry in a wide range of sedimentary rocks and fluids is as follows: Light (La, Ce, Pr, and Nd), Middle (Sm, Eu, Gd, Tb, Dy, and Ho), and Heavy (Er, Tm, Yb, and Lu) [12–15].

Historically, most REY reserves have been concentrated in carbonate igneous rocks, e.g., carbonatite as the enrichment process is a result of alkaline magmatism. Economically significant REY-rich formations are found in peralkaline igneous systems, magnetite–hematite bodies, iron–oxide–copper–gold (IOCG) deposits, monazite–xenotime-bearing placers, and ion-adsorption clay deposits [3,16]. Although REYs have mostly been mined from carbonatite bodies in the recent past, such as the Mountain Pass in California, local resources have been depleting too fast to meet the ever-increasing demand. On the other hand, China has been deemed the leading global producer of rare earths sourced from carbonatite bodies as well as ion adsorption clay-rich deposits [17–20]. To meet the exponential demand for REYs, research is being conducted to assess the possibility of REY recovery from sedimentary rocks such as coal and shale [21,22]. A few studies have suggested that REYs can be generated more conveniently from sedimentary rocks, giving them more economical and industrial appeal [23–25]. Sedimentary rocks are a highly utilized resource for oil, natural gas, and coal. Exploration of shale oil and gas generates large amounts of waste products, such as drill cuttings. Non-traditional sources of REYs from coal [22] and its combustion products [26–28] have contributed as major mined sources. Coal ash with elevated REY content has potential similar to that of conventional ores, such as carbonatites and alkaline granites [22,29].

Shale is a dark-colored sedimentary rock with varying proportions of silicates, carbonates, pyrites, oxides, organic matter, and detrital materials [30]. Each mineral phase contains elements associated with the crystal lattice or adsorbed to surfaces. Several processes can control REY enrichment in shales, such as (1) the source of detrital sediments; (2) bioaccumulation due to seawater upwelling; (3) input from fluvial/eolian systems; (4) oxidation reactions; (5) sulfidation during sedimentation; (6) microbial-mediated reactions at or near the surface; (7) diagenetic reactions or thermal maturation; (8) hydrocarbon migration; (9) intra-basinal brine migration; and (10) hydrothermal influx [31–42]. If the mineralogy of the shale is dominated by detrital flux, it generally shows a flat, normalized REY pattern, where the majority of the REYs present are adsorbed in the clay fraction [43]. However, this flat pattern can deviate if a particular mineral fraction gets enriched/depleted by any chemical or sedimentary processes. For instance, seawater upwelling can lead to high organic matter (e.g., phytoplankton). Since several REYs act as micronutrients for phytoplankton, phytoplankton can absorb a high amount of REYs, enriching the organic matter in REYs [35]. In euxinic depositional environments, sulfidation can occur, immobilizing REYs as sulfides [35,41]. Oxidation reactions, on the other hand, can form Fe–Mn (oxy) hydroxides, which also act as a sink for most REYs [36]. Diagenetic processes can lead to carbonate–phosphate precipitation and can enhance REYs in the carbonate–phosphate inventory [32,33,44]. Some other studies have observed that REY distribution in the clay fraction in shale may be modified by fluid alterations and associated chemical fractionation, e.g., by the influx of hydrothermal fluids [45–47]. Overall, these studies suggest that sources of sediments, depositional environments, diagenetic reactions, and fluid migration control the REY distribution in different fractions of shale.

Traditionally, REY patterns have been used to constrain the provenance and depositional environment of sedimentary rocks [23,48]. Such interpretations were based on the concept that the elemental behavior of REYs, which is dependent on chemical fractionation during the geochemical evolution of the rock, and a complementary distribution pattern is reflected in the fluid phases (e.g., [49–52]). For example, the redox-sensitive behavior of Ce and Eu makes these elements effective markers for studying redox processes. Ce³⁺ changes to Ce⁴⁺ and precipitates as CeO₂ as anoxic groundwater gets oxidized when discharged to the earth's surface [53,54]. On the other hand, Eu is present as Eu²⁺ in strongly

reducing hydrothermal fluids and associated sediments at mid-oceanic spreading centers, characterized by strong positive Eu anomalies relative to average shale Eu content [36,55].

The primary purpose of this study was to evaluate REY content and phase associations in two black shale basins, namely, Marcellus and Haynesville, with TOC ranging from 2.8 to 9 wt.%. Little is known about the REY-generating potential and their phase associations in these shales. This paper discusses obtained data on REY content in the whole-rock and mineral phases extracted via sequential leaching. The study also evaluates the REY extraction efficiency, highlights the limitations of current sequential extraction techniques, and suggests ways to improve them.

2. Materials and Methods

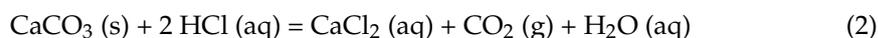
Sample selection: Three shale samples were selected for this study: one from the Marcellus basin (MIP-3H) and two from the Haynesville basin (1Ha and 5Hb). Sample selection was designed to compare the REY concentrations and extraction efficiencies in shales with different TOC contents and deposited in different environments during different geological time periods. The Marcellus Shale was deposited during the Middle Devonian and is located in the eastern and northeastern region of North America, covering Pennsylvania, Ohio, New York, West Virginia, and smaller parts of Kentucky, Tennessee, Maryland, and New Jersey. Marcellus Shale deposition was controlled by the Acadian Orogeny [56]. Black- and gray-colored shales accumulated in relatively deeper marine waters due to terrigenous input from mountain-building and subsequent erosion [57,58]. The Haynesville Shale was formed in the Jurassic period in southern parts of North America, namely southwest Arkansas, northwest Louisiana, and east Texas, and was deposited in a restricted basin located on a southward-sloping continental shelf under relatively shallow waters [59]. The mineralogical and organic matter of Haynesville Shale reflects a mixed accumulation of carbonate-dominant sediments generated within the basin that had a supply of clastic sediments. The restricted nature of the basin resulted in frequent anoxic conditions. The TOC content varies with the interplay of local carbonate input, changes in bottom-water anoxia, and dilution by clastic inputs [60,61].

Total organic carbon analysis: The total organic carbon contents of samples MIP-3H (sample from Marcellus basin), 1Ha, and 5Hb (samples from Haynesville basin) were calculated by measuring parameters S1, S2, and S4 using a source rock analyzer (SRA) in the IsoBioGem Lab. The procedure is outlined in Agrawal and Sharma, 2018b [62]. Briefly, 80 mg of powdered sample (75 microns) was isothermally heated at 300 °C for 3 min, liberating free hydrocarbons, which were detected in the FID as S1 (reported in milligrams). Following that step, the temperature was increased steadily from 300 to 600 °C. During this period, kerogen-bound hydrocarbons were liberated and detected as S2 (as milligrams per gram of rock). Residual organic carbon was measured as S4. WFT Source Rock Standard 533 (P/N 810-141) was used as a standard and run after every five samples. The standard deviations of S1, S2, S3, and TOC were 0.02, 0.5, 0.02 mg/g, and 0.09 wt.%, respectively. TOC was calculated as $0.1 \times (0.082 \times (S1 + S2) + S4)$ (in wt.%). The samples were then subjected to a sequential leaching experiment following a modified protocol outlined by Tessier et al., 1979 [63] and Riley et al., 2012 [64], and whole-rock analysis via the sodium peroxide fusion method (USGS Method 18, 2019).

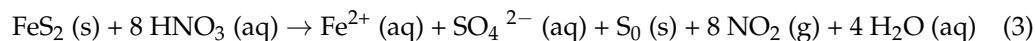
Sequential leaching procedure: A total of 11 g of sample was crushed and homogenized to 75 microns. The sample was added to 220 mL borosilicate beakers, and then a series of leaching steps were conducted to sequentially extract the major mineral fractions and organic matter associated with shale. At the beginning and between each leaching step, samples were washed with DI water for 18 h. After each leaching step, the supernatant liquid was filtered with 0.45 µm Millipore filters. The exchangeable phase was extracted with 88 mL of 1 M sodium acetate (Equation (1)), followed by continuous agitation on a shaker for 18 h at room temperature.



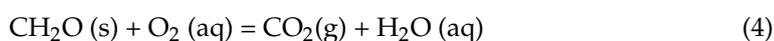
The residue was then treated with 165 mL of 6 M hydrochloric acid and allowed to roll for 18 h at room temperature to target the carbonates and oxides (Equation (2)).



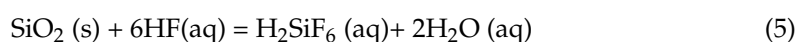
The next step was targeted to dissolve the pyritic (Equation (3)) and phosphatic phases using 165 mL of 2 M nitric acid for 18 h at room temperature.



Following the pyrites, the organically associated elements were extracted using 33 mL of 0.02 M nitric acid and 55 mL of 30% hydrogen peroxide (adjusted to pH 2). The mixture was heated to 85 °C with occasional agitation. Then, another 33 mL of hydrogen peroxide (pH 2) was added and agitated for 3 h (Equation (4)).



After cooling, 55 mL of 3.2 M ammonium acetate in 20% (*v/v*) nitric acid was added. The sample was diluted to 225 mL and agitated continuously for 30 min, and then the mixture sat for 48 h to allow the reaction to complete (after agitation and 24 h, effervescence was observed in all the samples; hence, the reaction time was extended to 48 h). After collecting the supernatant, the samples were transferred to conical 500 mL polypropylene flasks. Finally, the silicate minerals were extracted by adding 27.5 mL of concentrated hydrofluoric acid, i.e., HF (Equation (5)), and 2.75 mL of concentrated hydrochloric acid at 50 °C in a heated bath for 2 h and then diluting it to 165 mL with DI water.



Extra care was taken while handling HF. The mixture was allowed to sit on the hotplate overnight. Finally, 30 mL of the supernatant was transferred to a 100 mL Teflon beaker. The aliquot was neutralized with boric acid and was filtered using 60 mL Luer-Lok syringes to which 0.45 µm PVDF filters were attached (25 mm diameter) to collect the aliquots in precleaned 50 mL polypropylene centrifuge tubes, which were sent for analyses. After collecting 50 mL of aliquots at the end of each leaching step, the samples were diluted with 1% (of the total sample volume) concentrated nitric acid with Eppendorf micropipettes to prevent chemical deterioration.

Acid digestion of samples: About 5 gm of each powdered shale sample was used for the digestion of whole rock by the sodium peroxide fusion method. The procedure was carried out at NRCCE, West Virginia University. This was followed by measuring whole-rock concentrations of REYs.

Elemental analyses: For analyzing the 50 mL of acidified leachates and whole-rock concentrations, EPA methods 200.7 [65] and a modified 200.8 [66] were employed to measure major and trace element concentrations, respectively. These steps were taken to ensure analytical accuracy and reproducibility following QA/QC protocol. The instrument was run daily with four points and a blank along with a positive and a negative check. The positive check was to ensure recoveries were proper. The negative check (or the continuing blank) was performed to ensure that the blank was below the method detection limit (MDL). Check standards were run after every 10 injections to ensure that the analytical uncertainty was within $\pm 10\%$ for the Calibration Verification standard, and Calibration Blank standards were run every 10 samples. Each batch of 20 samples had a batch Blank and Laboratory Control Spike in addition to one sample run in duplicate. The MDLs (method detection limits) for the elements were as follows (in µg/L): Sc: 0.037, Y: 0.004, La: 0.003, Ce: 0.008, Pr: 0.003, Nd: 0.008, Sm: 0.004, Eu: 0.003, Gd: 0.003, Tb: 0.002, Dy: 0.004, Ho: 0.002, Er: 0.004, Tm: 0.002, Yb: 0.002, and Lu: 0.002. REY concentrations were measured in ICP-MS Nex ION 2000, Perkin Elmer 2018. Major elements such as Al were measured in ICP-OES 720 Agilent 2014, with an MDL of 0.059 mg/L.

XRD analysis: Unreacted and residual samples of 1Ha and MIP-3H were comminuted to 37 microns to identify mineralogical phases remaining after the sequential extraction procedure. This was done using a Siemens D500 diffractometer at the Pittsburgh Mineral and Environmental Technology (PMET) Lab. The crystalline phases were identified using SEM with energy-dispersive X-ray analysis to detect major and minor elements. Subsequent identification of crystalline phases was carried out using search-match software and quantified using Rietveld whole-pattern refinement. The samples were logged, identified, prepared, and analyzed according to PMET's Standard Operating Procedures.

3. Results

Bulk rock: In this study, experiments were performed on three samples: two from Haynesville (1Ha and 5Hb) and one from Marcellus (MIP-3H). The samples were selected such that their REY contents and extraction efficiencies could be assessed over a wide range of total organic carbon (TOC). The bulk concentration of each element and the total REY are given in Table 1; 1Ha-R (replicate) had the highest total REY content, i.e., 342.67 ppm, followed by 311.4 ppm in 5Hb and about 295 ppm in MIP-3H (Figure 1). To help us understand the patterns in the whole rock, the individual mineral fractions, and the geochemical processes of REY enrichment, we classified the elements into three groups: Light REE (LREE—La, Ce, Pr, and Nd); Middle REE (MREE—Sm, Eu, Sc, Gd, Y, Tb, Dy, and Ho); and Heavy REE (HREE—Er, Tm, Yb, and Lu), which is the scheme used by Yang et al., 2017 [41], but we also included Sc and Y in the discussion. Therefore, we use REY to refer to lanthanides plus Y and Sc, and REE when referring only to lanthanides.

Table 1. The concentration of each rare earth element (including Sc and Y) in whole-rock in ppm.

Sample	La	Ce	Pr	Nd	Sm	Eu	Sc	Gd	Y	Tb	Dy	Ho	Er	Tm	Yb	Lu	Total
1Ha	54.72	97.02	12.07	49.06	9.52	1.77	21.05	9.58	57.46	1.32	8.13	1.62	4.95	0.68	4.48	0.67	334.07
1Ha-R	56.68	99.53	12.61	49.61	9.42	1.75	22.25	9.79	58.71	1.33	8.29	1.63	5.11	0.72	4.54	0.70	342.68
5Hb	51.68	90.36	11.05	44.94	8.80	1.74	21.78	8.70	52.74	1.19	7.30	1.46	4.55	0.62	3.91	0.59	311.41
MIP-3H	38.68	72.35	10.41	46.27	10.06	2.26	21.25	11.24	56.66	1.58	9.51	1.94	5.74	0.81	5.13	0.76	294.64

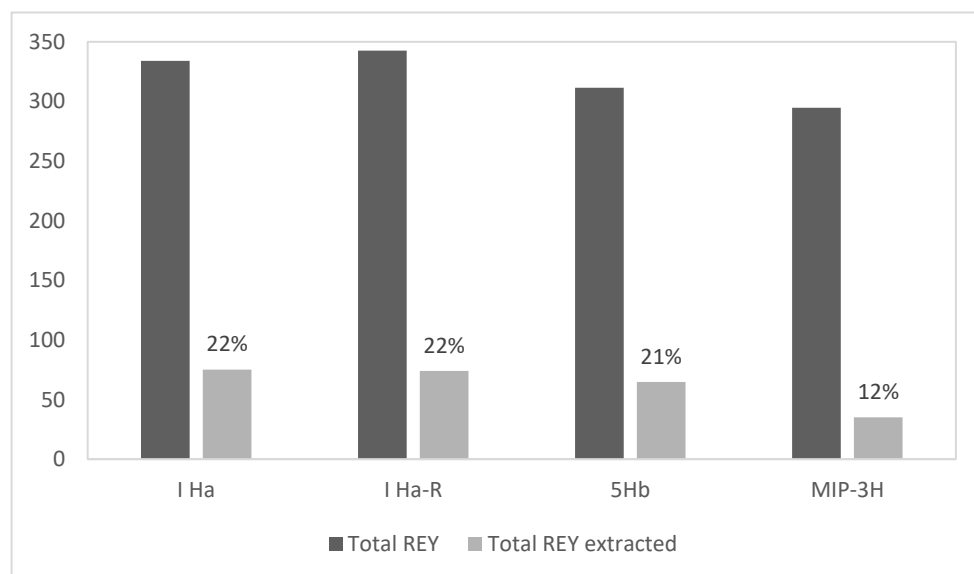


Figure 1. Total REY and amount extracted from the whole rock.

The TOC contents of 1Ha, 5Hb, and MIP-3H were 2.8, 3.4, and 9 wt.%, respectively. By convention, sample REY contents are normalized to a standard to facilitate comparison between local samples and global shale averages. There are two popular shales that represent global average REE contents, namely the Post Archean Australian Shale (PAAS) (Pourmand et al., 2012; Taylor and McLennan, 1985) and the North American Shale Com-

posite (NASC) (Gromet et al., 1984; Haskin et al., 1966). In this study, the sample REYs are normalized to NASC because they are better understood compared against an American shale. In addition, other parameters such as La/Lu, La/Sm, Gd/Lu, Ce/Ce*, Eu/Eu*, Y/Ho, and HREE/LREE that help understand the provenance, geochemical processes, and ore potential of the samples are also normalized to the corresponding NASC values (Figure 2). We notice the samples are about one to two times more enriched than the average shale composition. However, there is a distinct difference between the REY patterns of the Haynesville samples and the Marcellus samples. The Haynesville samples exhibit a relatively flat REY pattern, as indicated by similar values of La/Lu and Gd/Lu. On the other hand, the MIP-3H sample shows a moderately heavy REE-enriched distribution. Furthermore, Eu content is much less in the Haynesville region, which results in a distinctly different pattern than MIP-3H. Additionally, there is an apparent positive La anomaly in the Haynesville samples, whereas La is more depleted than the other light REEs in the MIP-3H Marcellus counterpart. Overall, we see a more uniform distribution of REYs in Haynesville Shale, and MREE enrichment in the Marcellus, followed by higher HREE than LREE. The five critical REYs [2], Nd, Eu, Y, Tb, and Dy, are at least 1.25 and 1.5 times more enriched in the Haynesville and Marcellus samples, respectively (Figure 3).

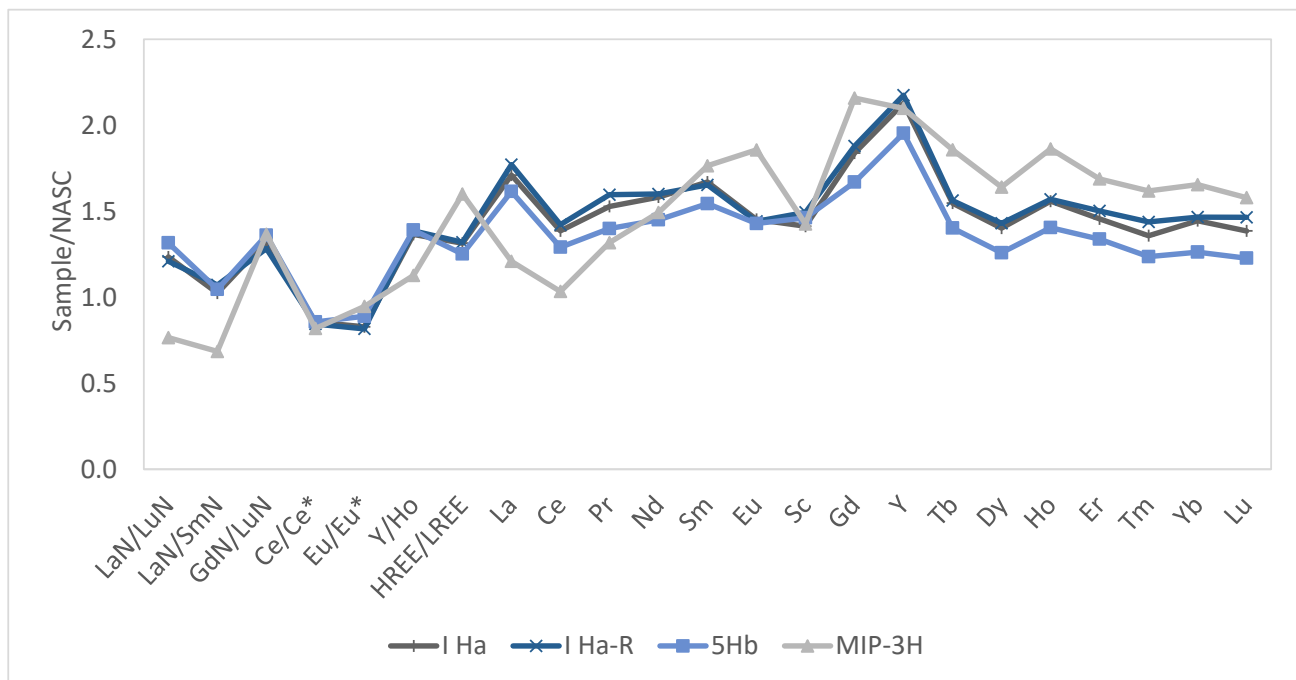


Figure 2. Whole-rock total REY distribution normalized to NASC and other indicators: La/Lu, La/Sm, Gd/Lu, Ce/Ce*, Eu/Eu*, Y/Ho, and HREE/LREE.

XRD: The mineralogical composition of the whole rock is given in Table 2. The MIP-3H sample is dominantly composed of quartz (46%), mixed clays (22%), calcite (16%), pyrite (11%), and some dolomite (5%). The 1Ha Haynesville sample has a few more mineral phases in addition to the above, except for mixed clays and dolomite. It is approximately 28.8% quartz and 39% plagioclase and mica minerals. Calcite (12%), gypsum (0.4%), and pyrite (1.5%) are also present. XRD analyses showed that both samples are dominantly composed of silicates. Post-reaction XRD of residual samples showed signs of precipitation of neo-fluoride silicates due to reaction with HF. Additionally, kalicinite (KHCO_3) was detected only in MIP-3H Marcellus Shale, which has a high TOC of 9%.

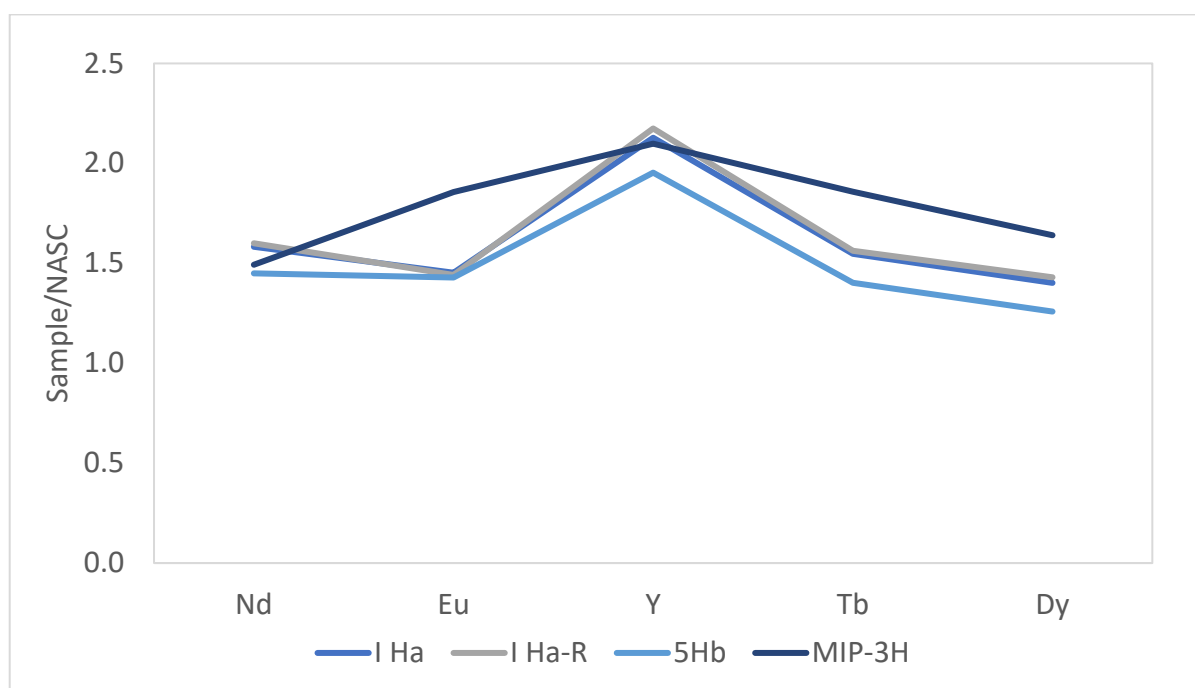


Figure 3. NASC-normalized whole-rock critical REY pattern.

Table 2. Mineralogy of unreacted 1Ha sample determined by X-ray Diffraction analysis and MIP-3H from Pilewski et al., 2019 [67].

Mineral Species (wt.%)	1Ha	MIP-3H
Quartz	28.8	46
Plagioclase	8.7	-
Mica	30.8	-
Mixed clays	-	22
Clinocllore	6.0	-
Kaolinite	8.1	-
Calcite	12.0	16
Dolomite	-	5
Gypsum	3.7	-
Rutile	0.4	-
Pyrite	1.5	11

Extracted fractions: The total REYs extracted from sequential extraction were about 75 ppm, 65 ppm, and 35 ppm in 1Ha, 5Hb, and MIP-3H, respectively (Figure 1). Based on whole-rock content, however, TREY content was significantly higher than the extracted REY concentrations. The concentrations of individual elements in each extract are given in Table 3. Nd, Er, Y, Tb, and Dy in the extracts are less than 0.8 times enriched compared to the average shale composite. However, this enrichment is only based on the ~20% of the total that was successfully leached. Figure 1 shows the extent of extraction from each sample: 1Ha, with the highest REY content, generated only 22%, followed by 21% from 5Hb and only 12% from MIP-3H. Compared to the REY contents, the extraction efficiency was the poorest for Marcellus shale. It is important to note that, although the extraction efficiency is low, we assume the REY distribution in the extracted fractions is representative of the mineral fractions in the whole rock. This assumption is based on numerous studies that have reported the association of a significant REY fraction with silicates, especially clay minerals, that are typically difficult to dissolve. Figure 4 shows the % of LREE (La–Nd), MREE (Sm, Eu, Sc, Gd, Y, Tb, Dy, and Ho), and HREE (Er, Tm, Yb, and Lu) extracted from each sample. The extraction of HREEs was relatively better for all samples, although

the HREE content was the lowest of all. Figure 5 shows the distribution of REYs in each leachate fraction. More than 93% of the extracted REYs in the whole rock are concentrated in the acid-soluble phase from the Haynesville samples and about 79% from the Marcellus sample (Figure 5). The REYs contributed by the exchangeable phase are negligible. Figure 6 shows the percent contribution of REYs extracted from each phase, indicating that about 9 to 22% of the entire REYs were extracted from the acid-soluble phase. MIP-3H has only a 2% contribution from the pyrite, organic, and silicate phases.

Table 3. Concentrations of each REY in each leachate in ppm.

Sample	La	Ce	Pr	Nd	Sm	Eu	Sc	Gd	Y	Tb	Dy	Ho	Er	Tm	Yb	Lu	Total
<i>1Ha</i>																	
Exch	BDL	BDL	BDL	BDL	BDL	BDL	BDL	BDL	BDL	BDL	BDL	BDL	BDL	BDL	BDL	BDL	0.02
Acid-sol	7.32	14.33	2.50	13.72	4.80	0.86	3.52	4.45	14.86	0.55	2.88	0.47	1.14	0.12	0.65	0.09	72.27
Pyr	0.12	0.20	0.04	0.21	0.06	0.01	0.09	0.06	0.30	0.01	0.05	0.01	0.03	BDL	0.02	BDL	1.21
Org	0.03	0.07	0.01	0.11	0.03	0.01	0.15	0.03	0.13	BDL	0.03	0.01	0.02	BDL	0.01	BDL	0.63
Sil	0.02	0.07	0.01	0.04	0.01	BDL	0.66	0.01	0.05	BDL	0.01	BDL	0.01	BDL	0.01	BDL	0.91
Total	7.49	14.67	2.56	14.08	4.91	0.88	4.43	4.55	15.35	0.56	2.97	0.49	1.20	0.13	0.68	0.09	75.04
<i>1Ha-R</i>																	
Exch	BDL	BDL	BDL	BDL	BDL	BDL	BDL	BDL	BDL	BDL	BDL	BDL	BDL	BDL	BDL	BDL	0.01
Acid-sol	7.27	14.27	2.50	13.59	4.72	0.85	3.46	4.47	14.87	0.55	2.86	0.47	1.15	0.12	0.63	0.09	71.87
Pyr	0.11	0.19	0.04	0.20	0.06	0.01	0.10	0.06	0.30	0.01	0.05	0.01	0.03	0.00	0.02	BDL	1.18
Org	0.01	BDL	BDL	BDL	BDL	BDL	BDL	BDL	BDL	BDL	BDL	BDL	BDL	BDL	BDL	BDL	0.01
Sil	0.02	0.07	0.01	0.04	0.01	0.00	0.67	0.01	0.05	0.00	0.01	0.00	0.01	0.00	0.01	BDL	0.91
Total	7.41	14.54	2.54	13.83	4.79	0.86	4.23	4.53	15.22	0.56	2.91	0.49	1.18	0.12	0.65	0.09	73.98
<i>5Hb</i>																	
Exch	BDL	BDL	BDL	BDL	BDL	BDL	BDL	BDL	BDL	BDL	BDL	BDL	BDL	BDL	BDL	BDL	0.01
Acid-sol	6.83	12.32	2.23	13.03	4.44	0.92	2.44	4.24	9.07	0.55	3.00	0.50	1.27	0.14	0.78	0.11	61.88
Pyr	0.09	0.15	0.03	0.16	0.05	0.01	0.08	0.05	0.27	0.01	0.04	0.01	0.03	BDL	0.02	BDL	0.99
Org	0.05	0.10	0.02	0.16	0.05	0.01	0.22	0.05	0.21	0.01	0.05	0.01	0.03	BDL	0.02	BDL	0.97
Sil	0.05	0.12	0.01	0.06	0.01	BDL	0.61	0.01	0.04	BDL	0.01	BDL	0.01	BDL	BDL	BDL	0.92
Total	7.02	12.69	2.30	13.40	4.54	0.94	3.35	4.34	9.58	0.57	3.10	0.52	1.34	0.14	0.82	0.11	64.77
<i>MIP-3H</i>																	
Exch	BDL	BDL	BDL	BDL	BDL	BDL	BDL	BDL	BDL	BDL	BDL	BDL	BDL	BDL	BDL	BDL	0.02
Acid-sol	1.25	3.77	1.08	7.42	3.58	0.74	0.70	3.34	2.03	0.37	1.78	0.28	0.68	0.07	0.43	0.06	27.59
Pyr	0.04	0.13	0.03	0.28	0.26	0.07	0.14	0.28	0.70	0.05	0.35	0.06	0.18	0.02	0.14	0.02	2.76
Org	0.04	0.10	0.02	0.18	0.26	0.08	0.17	0.28	0.69	0.05	0.35	0.06	0.17	0.02	0.14	0.01	2.63
Sil	0.11	0.29	0.04	0.17	0.07	0.02	0.53	0.08	0.36	0.01	0.11	0.02	0.08	0.01	0.09	0.01	2.03
Total	1.45	4.28	1.18	8.05	4.16	0.92	1.55	3.99	3.78	0.49	2.59	0.43	1.11	0.14	0.80	0.10	35.02

Note: BDL, Below Detection Limit; Exch, Exchangeable; Acid-sol, Acid-soluble; Pyr, Pyrite; Org, Organic; Sil, Silicate.

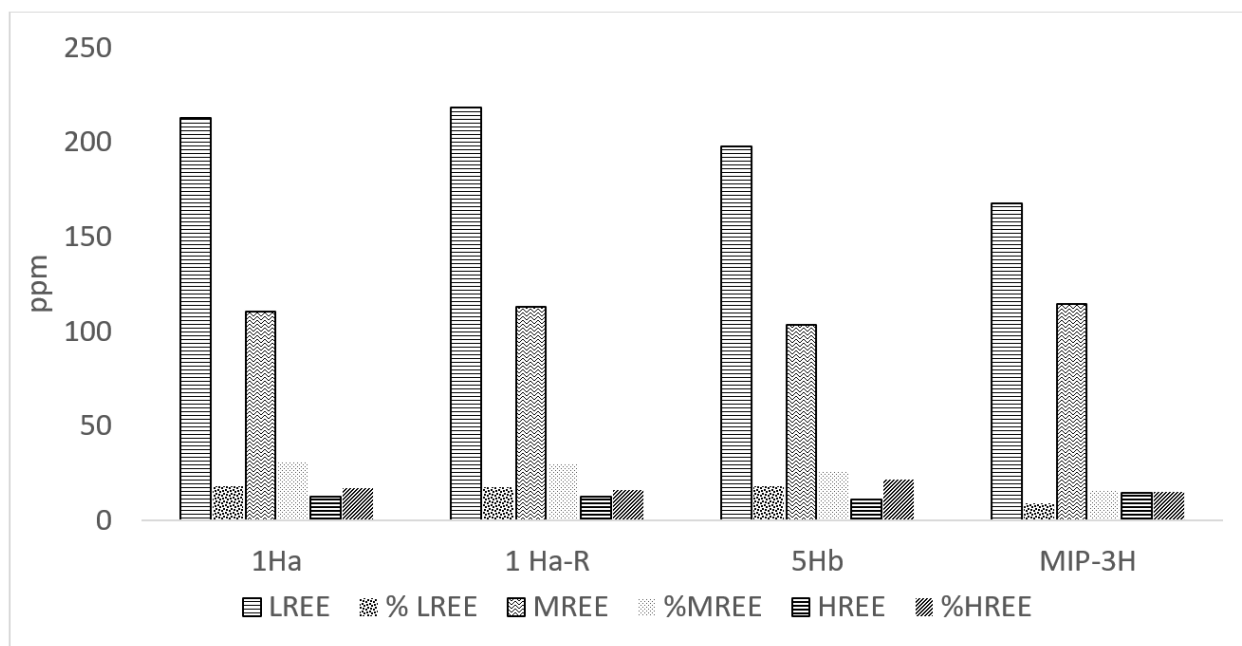


Figure 4. Concentration (in ppm) and percentage of LREE, MREE, and HREE fraction extracted.

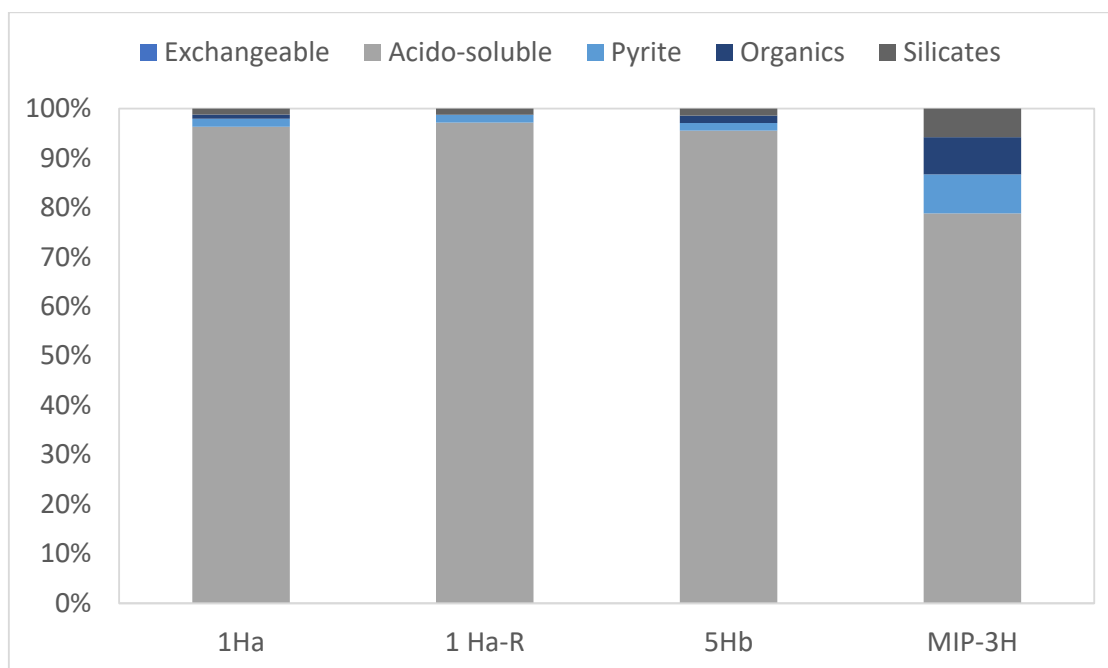


Figure 5. Total REY distribution in the extracted rock fractions.

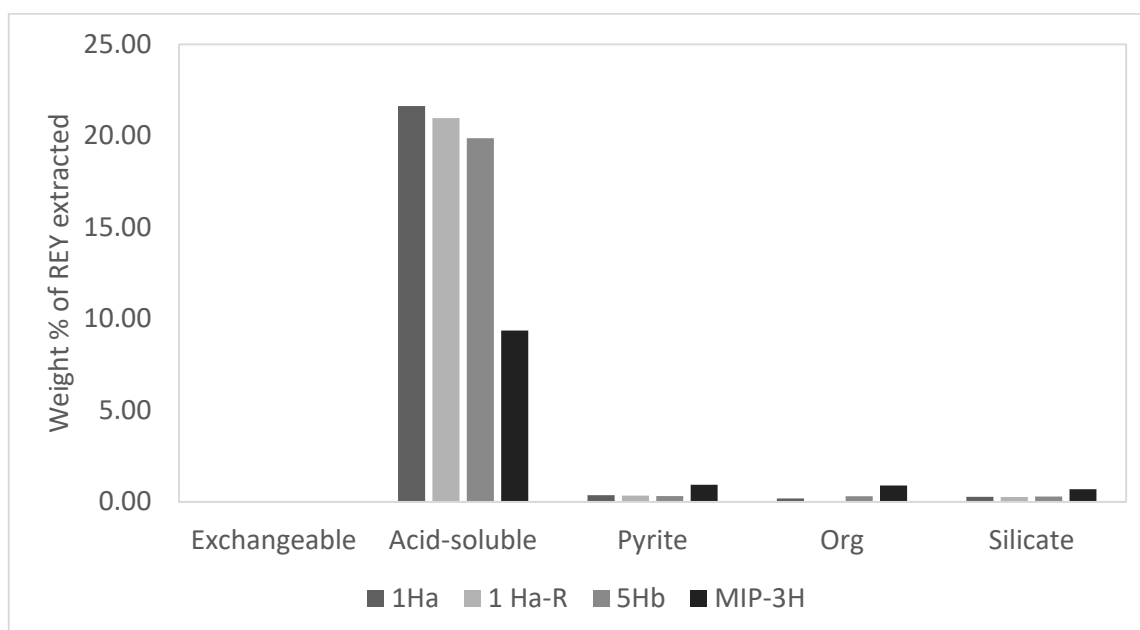


Figure 6. Percentage of REY extracted from each phase. The REY content in the residual matter was not determined.

4. Discussion

4.1. REY Distribution Patterns

REY signatures in the whole rock: 1Ha-R (replicate) had the highest total REY content of all, i.e., 342.67 mg/kg, followed by 334.07 ppm in 1Ha, 311.4 mg/kg in 5Hb, and 294.64 ppm in MIP-3H (Figure 1). The NASC-normalized REY distribution in the Marcellus and Haynesville shale samples was used to understand the extent of REY enrichment in the samples and to account for any significant anomalies. This enrichment pattern is confirmed by the La/Lu, La/Sm, and Gd/Lu ratios—La, Sm, and Gd being the indicators for LREE, MREE, and HREE, respectively (Figure 2). La/Lu and La/Sm ratios are

less than 1, suggesting that LREEs are depleted relative to both MREEs and HREEs. The Gd/Lu ratio is about 1.5, indicating higher MREE content than HREE. These values, on the other hand, are significantly different for samples 1Ha and 5Hb. Apart from Gd/Lu, the La/Lu and La/Sm values of about 1.25 and 1.1, respectively, indicate that the LREEs in the Haynesville Shale are slightly more enriched than the HREEs and the MREEs. These elemental ratios, therefore, indicate that the relative predominance of different rare earths in the samples are controlled by differences in mineralogical composition and/or geochemical processes driving preferential partitioning between the host fluid and the mineral phases, such as silicates, carbonates, phosphates, and Fe–Mn oxyhydroxides. Geochemical processes are better understood when the patterns are studied for individually extracted phases from rock. A study on Devonian and Jurassic black shale revealed possible REY associations with (i) authigenic phases of carbonate and phosphate phases or (ii) refractory organic matter and siliciclastic minerals [40]. Ancient black shale may have undergone a diagenetic transformation that resulted in the formation of authigenic minerals such as authigenic carbonate, fluorapatite, or bioapatite. REEs are found to be highly enriched in these authigenic phases. Moreover, these minerals usually exhibit middle-to-heavy REE enrichment, as seen in our samples as well. A study by Yang et al., 2017 [40] showed that prominently MREE-enriched REYs on the whole point towards the presence of detrital apatite and calcium fluorapatite (CFA). Our data point towards dominant MREE enrichment in all three samples, but there is also a combined presence of HREEs. XRD data reveal that CFA and apatite were not detected in whole-rock. However, the overall MREE–HREE pattern suggests that the influence of siliciclastic and carbonate phases may be more significant in our study.

Several hypotheses have been proposed for HREE-enriched signals. At the sediment-water interface, HREE-enriched signals could predominantly result from preferential particulate scavenging of LREEs by organics. Further, several studies suggest stronger complexation bonds are formed between HREEs and carbonates, which could lead to HREE enrichment in shale [12,68–72]. Another model to explain HREE-enrichment in whole-rock is the interaction of deeper methanogenic sediments with HREE-enriched porewater [73] at higher alkalinity, resulting in more stable dissolved complexes between HREE and the carbonate ligands [74–76]. However, in shales that are not diagenetically altered, REYs are generally concentrated in refractory organic matter and siliciclastic fractions.

The REY enrichment in our samples could be explained by REY association with phosphorites [24,77], clay minerals [78], organic matter [21] or hydrothermal mineralization [22]. The high REY content in our samples could plausibly be related to syngenetic reactions in an anoxic environment or post-depositional influences [21,79].

XRD analyses indicate that the major mineral phases in our samples are silicate minerals. The residual matter after leaching shows a high % of undissolved silicates. Therefore, we hypothesize that the unextracted REY is associated with refractory silicates. Within silicates, clays are one of the primary hosts of REYs, and several other trace elements [78,80] reported a strong statistical correlation of Al and Si with REYs. Al and Si are also mostly found in the crystal lattice of silicates, especially clays (such as kaolinite, smectite, and illite). Clays can host REYs in the interlayer spaces and/or at the edges and surfaces due to their unique properties such as high permanent surface negative charge and high surface-to-volume ratios [78,81]. REYs can be incorporated into clay during mineralization/weathering and can therefore be attributed to provenance. REYs can also become preferentially partitioned into clays during riverine transport or be adsorbed to surfaces from seawater. Further, the association of trace elements with Al and Si is only governed by a limited number of processes, as they are not sensitive to redox changes (Xu et al., 2018).

Additionally, bulk Al content was measured to calculate REY/Al in samples 1Ha, 5Hb, and MIP-3H. Al was used as a proxy for detrital material in 28 core samples collected from MIP-3H, and the detrital-dominated REY signature was indicated by a TREY/Al value of 0.0025 ± 0.006 . In our samples, TREY/Al (whole rock) ranges from 0.0044 to 0.0052, which is at least 1.7 times more than the average of the 28 detrital-dominated Marcellus

samples [44]. Additionally, we note HREE enrichment in all the samples relative to LREEs. These results suggest that samples have detrital sources that were more enriched in REE as compared to the Marcellus samples from Phan et al., 2019 [44], suggesting more REE were adsorbed to clays. HREE enrichment could also potentially indicate an influx of other sources, such as organics or inorganic fractions that preferentially retain HREEs. TREY/Al values indicate a moderate-to-high influx of detrital matter during the deposition in the Marcellus and Haynesville basins. Based on the LREE and trace-element profiles, it has been interpreted that the organic-rich zone in the Marcellus basin was formed in a magmatically quiescent period [82]. Studies have also shown evidence of alternating suboxic and anoxic redox conditions controlled by finer-scale tectophases during the active-mountain-building phase of the Acadian orogeny during Marcellus deposition [62,83–87]. These events might have led to minor fluctuations in detrital input and influenced REY variations. However, more spatiotemporal data are needed from different parts of the Marcellus Basin to better understand these relations. There may be similar modes of occurrence in the Haynesville basin, but little is known about the subtle variations in geochemical parameters. Our data suggest that the provenance and geochemical processes in the Haynesville Shale basin are different from the Marcellus Shale basin, resulting in differences in mineralogy, TOC, and REY concentrations. However, more high-resolution data and research are warranted to better understand spatiotemporal variations

REY signatures in the extracted phases: We see a predominantly middle-REE-enriched pattern in the extracted phases from the leaching experiment (Figure 7). To delineate the MREE enrichment pattern, we sought to observe the REY distribution in each of the extracted phases. The exchangeable phases, in which the REY concentrations were less than 0.001 $\mu\text{g/L}$, are not considered in this discussion. We see an MREE enrichment pattern in the acid-soluble, pyritic, and organic extracts, but HREE enrichment in the silicate leachate. However, Tb, Y, and Sc concentrations were much lower than the concentrations of the rest of the lanthanides, indicating that extraction of these three elements was extremely poor (Figure 8). The presence of Fe–oxyhydroxides can result in MREE enrichment in these phases [73,88–90]. However, this is unlikely, as these shales were deposited in anoxic to euxinic environments, and the competing influence of REE associated with carbonates, phosphates, or organic matter is more likely than with oxy–hydroxide coatings [67,83,91–97]. The other likely source of MREE enrichment could be authigenic minerals such as bioapatite and phosphate nodules [14,34,68,98]. Alternatively, the MREEs could be concentrated in the organic matter [92].

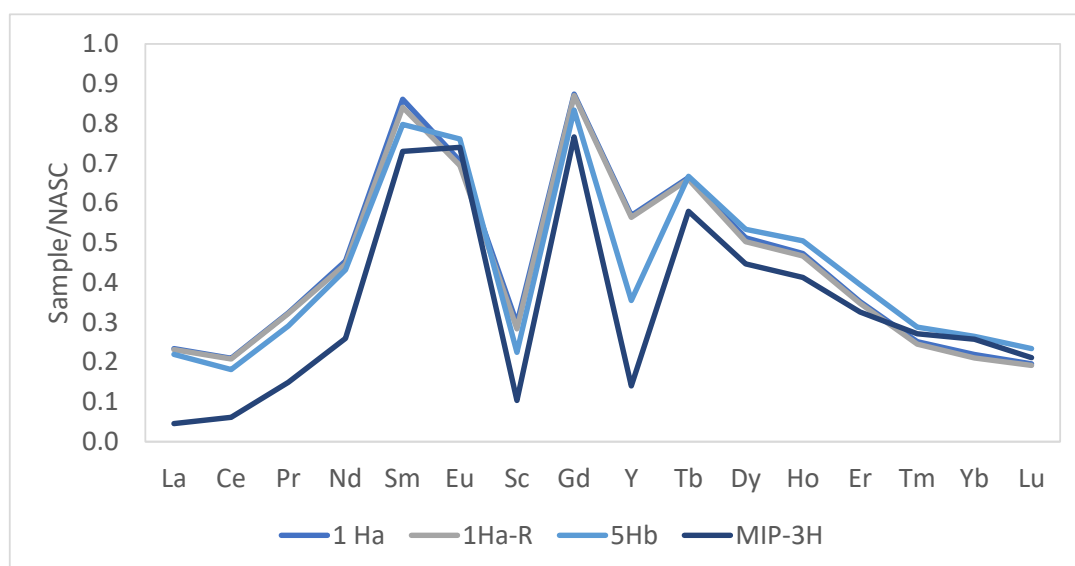
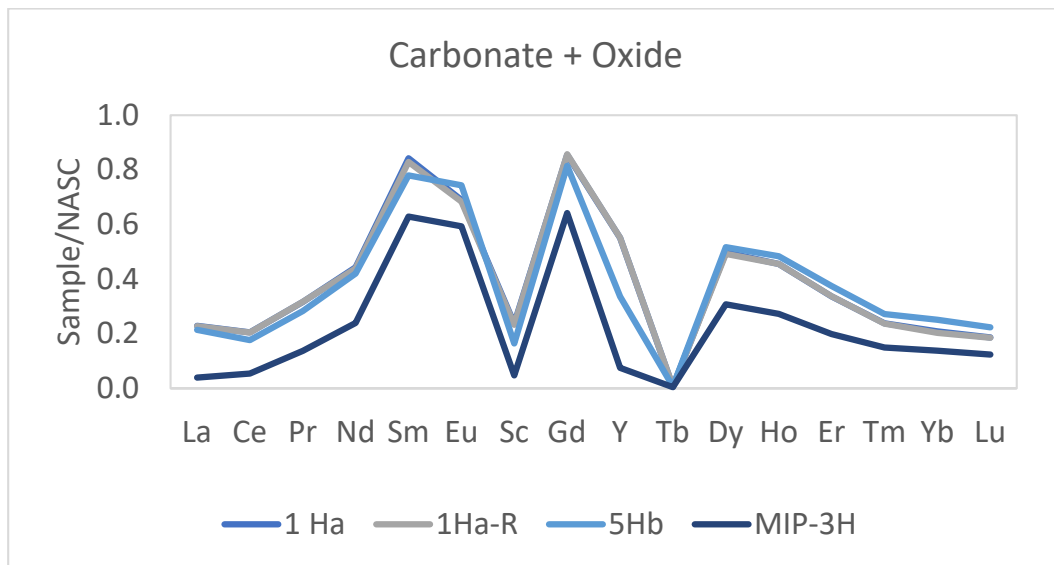
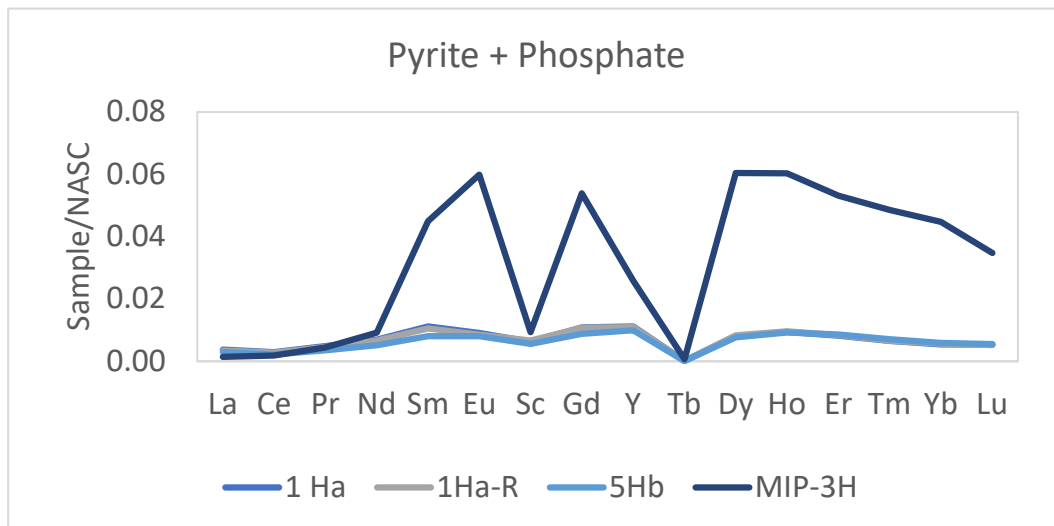


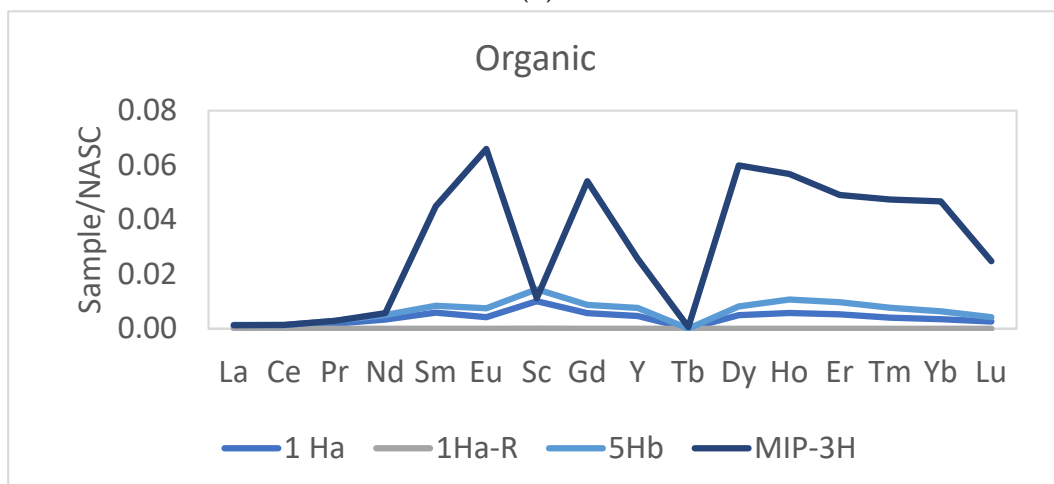
Figure 7. Extracted total REY pattern.



(a)



(b)



(c)

Figure 8. Cont.

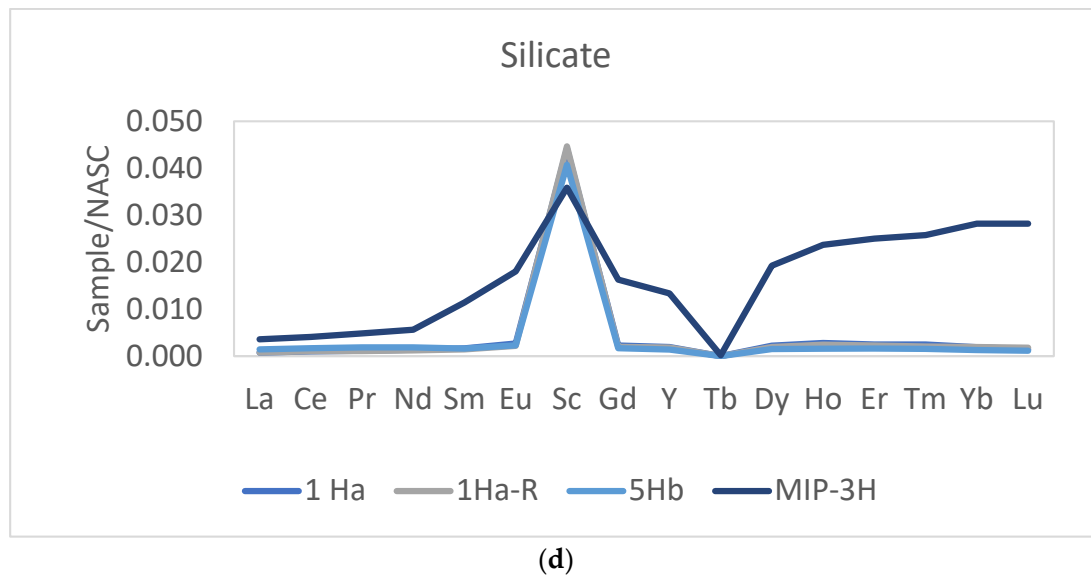


Figure 8. REY patterns in the mineralogical phases: (a) carbonate+oxide, (b) pyrite+phosphate, (c) organics, and (d) silicate.

The pronounced MREE enrichment in the acid-soluble phases indicates there may be a combined influence of carbonate complexation and precipitation of bioapatite or other authigenic phosphates (Figure 8a) [12,14,15,34]. The acid-soluble step of the experiment was designed to target the carbonates and oxides, and the pyrite-dissolution step targeted pyritic and phosphatic minerals. Since both these steps involved strong acids, REY data in both these phases may indicate phosphate mineral dissolution [44]. One study reported that MREE enrichment in carbonates and the organic-matter fraction of Marcellus Shale could potentially be due to the interaction between diagenetic pore fluid and organics during diagenesis that later crystallized to form carbonate cement [95]. We observe consistent MREE enrichment in the carbonates and pyrites (phosphates included) suggesting that our samples have also undergone strong diagenetic alteration.

On the other hand, MREE enrichment in the organic matter could be due to a different process (Figure 8c). The light and the middle REEs are likely mobilized during anoxic diagenesis [40]. A comparison of REE patterns in ancient organic with that in freshly deposited organic matter shows MREE enrichment in the new organic matter [92]. The MREE- and HREE-enriched pattern in the organic phases in our study supports the hypothesis that microbial respiration of sedimentary organic matter might have released light REE over MREE into the pore water (e.g., [99]). However, it is unclear why HREEs may be mobilized under anoxic conditions. We postulate that enrichment may indicate the dominance of relatively newer organic matter in ancient black shales. It could also suggest localized differences in organic matter inputs in the depositional basin.

As for the silicate extract, we observe prominent HREE enrichment in MIP-3H and a relatively flat distribution for the Haynesville samples (except for Tb) (Figure 8d). The observation for MIP-3H is expected, as we observe the dominance of MREEs in carbonates, phosphates, pyrites, and organics. Additionally, our whole-rock REE pattern indicates a modern seawater signature indicated by negative Ce anomalies, slightly chondritic Y/Ho ratios varying from 29–36, LREE depletion, and HREE enrichment [44]. The siliciclastic fraction should ideally balance the whole-rock REE content, which is also MREE-to-HREE enriched. Heavy REE dominance in the silicates could be due to hydrogenous inputs [12,15]. However, for the Haynesville shale, the whole REY pattern is much flatter and is representative of the average shale distribution. This difference indicates that the Haynesville and Marcellus Shale basins were subjected to different seawater inputs with different REE signatures. La enrichment and negative Eu anomalies in Haynesville whole-rock support our argument that the sources of REY enrichment are different for the two basins, although

both exhibit modern seawater signatures. Our study demonstrates that the extraction and subsequent distribution of REYs are strongly dependent on geochemical processes and the past depositional environment. This observation warrants further research to better understand the origin of REY patterns in two separate depositional basins.

4.2. Extraction Efficiency of REYs

The goal of our leaching study was to extract the exchangeable carbonates, oxides, phosphates, mono-sulfides, pyrite, organic matter, and silicate minerals to understand REY distribution in different phases. We followed the procedure outlined by Riley et al., 2012 [64] and extended the theory conceptualized by Tessier et al., 1979, which targets the above-mentioned phases. However, only 12–22% of the total REYs were extracted using this method (Figure 1). We anticipated the silicates should have undergone complete dissolution, as we extended the HF and HCl reaction times with the silicates from 2 h (as outlined in Riley et al., 2012 [64] to over 24 h. However, the increased reaction duration did not significantly affect the REY concentration in this leaching step. This is one of the drawbacks of performing sequential leaching based on operationally defined mineral phases that may not accurately represent the actual phases in the sample [40]. It would have been beneficial to determine the mineralogical composition and pXRF analysis of specific elements that tend to exhibit a higher degree of association with REYs, such as P, Al, Mo, Zn, Ni, U, Fe, and S, before designing the leaching procedure [21]. Additionally, we argue that traditional leaching methods may not be a robust strategy for building geochemical models of REY associations in marine shale mineral constituents.

Few studies have focused particularly on REY extraction from ancient black shales [40,44]. They used different leaching methods, considering that the target fractions in each study were different. Yang et al., 2017 [40] used a modified sedimentary extraction (SEDEX) procedure [100] to measure phosphorus levels in different mineral fractions, namely reducible, authigenic, detrital, and organic fractions, as outlined in Anderson and Delaney 2000 [101]. Although the extraction efficiency of REEs was significantly high (almost 80% in many samples), there was still an “unrecoverable” fraction remaining at the end of the procedure [40]. This residue is postulated to be refractory siliciclastic material. Phan et al., 2019 [44] performed sequential leaching using three separate procedures that were designed to target the following: Procedure I targeted the inorganic phases (water-soluble, exchangeable, and completely dissolved carbonates and phosphates); Procedure II (water-soluble, exchangeable, and partially dissolved carbonates and phosphates); and Procedure III (long-chained, unbranched aliphatics, and short-chained, highly branched aliphatics). The residues constituted organic matter, sulfides, and siliciclastics at the end of Procedures I and II, with II containing the undissolved carbonates. We calculated the extraction efficiency of the inorganic leaching procedures outlined by Phan et. al., and the REYs extracted from the bulk rock averaged around 20%–25%, with a few exceptions. The Marcellus samples, which had an average carbonate content of 15 wt.%, yielded 39 to 54% of the total REEs in the whole rock. On the other hand, Tully Limestone samples that contained more than 70% carbonate by weight yielded almost 65 to 84% of the total REEs. Interestingly, one of the carbonaceous shale samples that contained 7.4% TOC and 15.6% carbonates yielded only 36% of the total REEs [44]. The Marcellus sample used in our study contained 16% calcite and 9% TOC, so it can be classified as carbonaceous shale. Our REY results indicate that 12%–15% carbonate content is likely not the only factor controlling REY yield. Organics can also play a key role in impacting the REY yield. Incomplete removal of organic carbon in the organic-leaching step can also hinder REY yield. We see evidence of precipitation of kalicinite in the post-reaction Marcellus sample, suggesting recrystallization of bicarbonate minerals due to incomplete removal of organic carbon in the organic-leaching step [102]. Kalicinite is precipitated when CO₂ is released and gets protonated to form a bicarbonate molecule and further bonds with potassium ions in solution. The reason we did not observe kalicinite in the Haynesville sample could be due to the complete removal of organics because of the relatively lower TOC content. We hypothesize that REY extraction efficiency

could potentially be higher in samples with high carbonate content (>10%) but with TOC less than 8% using the current leaching protocol. A previous study also observed lower REE levels in high-TOC samples [103]. Therefore, we postulate that, along with mineralogy, both the TOC and carbonate contents should be taken into consideration for improving REE yield.

Developing a better understanding of the formation and geochemical behavior of refractory residual matter is crucial to determine the origins of REY signatures in the whole rock. There is also a need to develop new extraction techniques that can help target REYs in organic-rich and silicate-dominant black shales. Possible techniques include changing the rock-to-extractant ratio and/or adjusting the reaction temperatures and duration of contact between rock and fluid. A preliminary attempt at modeling a suitable reaction time to recover 90% of the elements from the carbonate fraction shows that the ideal duration can be as high as 600 h, holding all other parameters constant (unpublished model). It was found that the rate of acid leaching increased after the first 80 h and plateaued around 450 h. Additionally, in order to target specific phases, more-efficient chemical reagents may help improve the yield. For example, using strong oxidizers can degrade organic matter, including kerogen, which is an insoluble organic compound in shale [104,105]. Silicates are generally difficult to dissolve, but reagents such as sodium carbonate and sodium hydroxide have been used to dissolve coal fly ash with >90% efficiency [106,107]. Other techniques could include the peroxide-based fusion to convert the silicate-rich residual matter.

4.3. Evaluating Shale Samples as a Potential REY Source

The problem with assessing shale as a potential REY source is that the standards of economic assessments are based on industrial cut-offs for ore deposits or average REY contents in coal byproducts. Seredin and Dai 2012 proposed a method for evaluating the economic recovery of REY from coal and coal byproducts. For REY from combustion wastes (Russian Far East Coals) to be considered for beneficial recovery, 0.1% REY in ash was the cut-off grade before pre-crisis times. For coal benches greater than 5 m thickness having rare earth oxides ≥ 1000 ppm, the cut-off grade could be lowered to 800–900 ppm REO, which is about 721 ppm REY. The total REY in the shale samples in our study ranged from 294.64 ppm in MIP-3H to 342.68 ppm in 1Ha-R and 311.41 ppm in 5Hb samples. We see higher TREYs in Haynesville shale than in Marcellus shale. To explore newer, unconventional REY sources such as shale waste, we need to develop revised economic cut-offs. In a Sichuan shale basin, researchers were able to recover up to 189 $\mu\text{g/L}$ of Europium from produced waters [108]. Our results show that with enhanced recovery protocols, shales such as Haynesville and Marcellus can recover as much as 200 $\mu\text{g/L}$ of REYs, assuming the mineralogy and TOC content of the samples are within the ranges that allow optimal yield.

One indicator for estimating the REY resource potential of shale could be the HREE-to-LREE ratio. Heavy REEs are relatively rarer than LREE, and therefore, a high HREE-to-LREE ratio indicates higher REE recovery potential from the deposit. In our samples, we see a lower HREE+Y/LREE for whole-rock ranging from 0.06–0.09 and an even lower ratio in the extracted portion, ranging from 0.05–0.14. A notable fact is that in both cases, the MIP-3H sample had the lowest TREY content but the highest ratios in both the whole-rock and extracted portions. A similar observation was made for coal samples [21].

Another approach to determine the REY potential of these samples could be assessment with respect to the contribution of critical REEs [109]. This parameter is called the “outlook coefficient” (C_{outl}) and is calculated as $C_{\text{outl}} = (\text{Nd} + \text{Eu} + \text{Tb} + \text{Dy} + \text{Er} + \text{Y} / \text{SumREY}) / (\text{Ce} + \text{Ho} + \text{TM} + \text{Yb} + \text{Lu} / \text{SumREY})$. This equation was proposed to determine the REY potential of coal (ash basis). However, to apply this assessment to shale, we would need to consider the sample on a whole-rock basis [21]. Higher C_{outl} values would indicate a more-promising REY deposit of shale. In this study, the outlook coefficient in whole-rock ranged from 1.16 in Haynesville shale to 1.51 in the Marcellus sample, which is low to intermediate. Although the outlook coefficient could be an indicator of REY sources,

we need to consider that the availability of these elements is a function of demand and supply changes in the economy. Therefore, there is a need to modify the definition of a high outlook coefficient in response to changes in market trends. Further, most REY recovery studies are based on coal and post-combustion coal products. Therefore, more research is warranted to develop robust models for predicting shale REY potential.

5. Conclusions

This study reports the feasibility of REY recovery from black shale, particularly from the Marcellus and the Haynesville basins in the US. The main findings of this study are as follows:

- Whole-rock REY content ranges from 295 to 342 ppm, and the highest recovery was from the acid-soluble shale fraction comprising carbonates, oxides, and phosphates.
- The whole rock exhibits an MREE-to-HREE-enriched pattern owing to the mineralogical controls and geochemical processes such as preferential incorporation of MREE in the carbonates and HREE in the clay and refractory fractions.
- The REY contributed by the exchangeable phase is negligible. About 9 to 22% of the entire REY was extracted from the acid-soluble phase. The MIP-3H Marcellus sample reported only a 2% contribution from the pyrite, organic, and silicate phases.
- The overall REY extraction efficiency was relatively poor because a major portion of the REYs were concentrated in mixed clays and refractory phases that were difficult to dissolve. The poor recovery could also be attributed to the concentration of REYs in refractory insoluble fractions, including silicates, or due to incomplete reactions. Other materials, such as pyrobitumen and kerogen, might also hold a significant amount of critical metals. However, the presence of these insoluble materials cannot be constrained by the leaching protocol used in this study.

This research potentially opens new avenues in understanding the fundamental mechanisms of REY enrichment in black shale. The study also highlights the need for developing new techniques to improve the extraction of REYs from shales of different mineralogies, maturities, and depositional environments. The development of scientific and engineering approaches to enhance REY recovery from oil and gas shale basins can help develop black shales as potential REY resources, contributing to improving the US economy while reducing its dependence on imports.

Author Contributions: Conceptualized the idea for this study V.A. and S.S.; Conducted the experiments S.B. and V.A.; Wrote the first draft of the manuscript S.B.; edited the manuscript V.A. and S.S. All authors have read and agreed to the published version of the manuscript.

Funding: This research was funded by the IsoBioGeM laboratory and Summer Graduate Research Grant by the Department of Geology and Geography at WVU, The APC was funded by WVU Open Access Author Fund.

Data Availability Statement: Not applicable.

Acknowledgments: We also appreciate the contributions of Bennington Opdahl, who helped design the experimental protocol, and Rachel Yesenchak for her assistance at the time of ongoing laboratory work and for sharing important insights.

Conflicts of Interest: The authors declare no conflict of interest.

References

1. Department of Energy (DOE). *U.S. Department of Energy Report on Rare Earth Elements from Coal and Coal Byproducts*; Report to Congress; Department of Energy (DOE): Washington, DC, USA, 2017; p. 20585. [CrossRef]
2. Burner, S. Rare Earth Element Database. National Energy Technology Laboratory, U.S. Department of Energy. 2017. Available online: <https://Edx.Netl.Doe.Gov/Ree/> (accessed on 5 August 2021).
3. Schulz, K.J.; DeYoung, J.H., Jr.; Seal, R.R., II; Bradley, D.C. (Eds.) *Critical Mineral Resources of the United States—Economic and Environmental Geology and Prospects for Future Supply*; U.S. Geological Survey Professional Paper 1802; U.S. Geological Survey: Reston, VA, USA, 2017; 797p. [CrossRef]

4. Grandell, L.; Lehtilä, A.; Kivinen, M.; Koljonen, T.; Kihlman, S.; Lauri, L.S. Role of critical metals in the future markets of clean energy technologies. *Renew. Energy* **2016**, *95*, 53–62. [[CrossRef](#)]
5. Kronholm, B.; Anderson, C.G.; Taylor, P.R. A primer on hydrometallurgical rare earth separations. *JOM* **2013**, *65*, 1321–1326. [[CrossRef](#)]
6. Mayfield, D.B.; Lewis, A.S. Environmental review of coal ash as a resource for rare earth and strategic elements. In Proceedings of the World of Coal Ash Conference, Lexington, KY, USA, 22–25 April 2013; Available online: <https://www.flyash.info/2013/051-Mayfield-2013.pdf> (accessed on 10 September 2021).
7. Blissett, R.S.; Smalley, N.; Rowson, N.A. An investigation into six coal fly ashes from the United Kingdom and Poland to evaluate rare earth element content. *Fuel* **2014**, *119*, 236–239. [[CrossRef](#)]
8. Franus, W.; Wiatros-Motyka, M.M.; Wdowin, M. Coal fly ash as a resource for rare earth elements. *Environ. Sci. Pollut. Res.* **2015**, *22*, 9464–9474. [[CrossRef](#)]
9. Scott, C.; Deonarine, A.; Kolker, A.; Adams, M.; Holland, J. Size distribution of rare earth elements in coal ash. In Proceedings of the World of Coal Ash Conference, Nashville, TN, USA, 5–7 May 2015.
10. Agrawal, V.; Sharma, S. Critical Minerals: Current Challenges and Future Strategies. *IJESNR* **2021**, *27*, 556215. [[CrossRef](#)]
11. Available online: <https://iea.blob.core.windows.net/assets/ffd2a83b-8c30-4e9d-980a-52b6d9a86fdc/TheRoleofCriticalMineralsinCleanEnergyTransitions.pdf> (accessed on 20 December 2021).
12. Chen, J.; Algeo, T.J.; Zhao, L.; Chen, Z.-Q.; Cao, L.; Zhang, L.; Li, Y. Diagenetic uptake of rare earth elements by bioapatite, with an example from Lower Triassic conodonts of South China. *Earth-Sci. Rev.* **2015**, *149*, 181–202. [[CrossRef](#)]
13. Deng, Y.; Ren, J.; Guo, Q.; Cao, J.; Wang, H.; Liu, C. Rare earth element geochemistry characteristics of seawater and porewater from deep sea in western Pacific. *Sci. Rep.* **2017**, *7*, 16539. [[CrossRef](#)]
14. Kidder, D.L.; Eddy-Dilek, C.A. Rare-earth element variation in phosphate nodules from Midcontinent Pennsylvanian cyclothem. *J. Sediment. Res.* **1994**, *64*, 584–592.
15. Zhang, L.; Algeo, T.J.; Cao, L.; Zhao, L.; Chen, Z.-Q.; Li, Z. Diagenetic uptake of rare earth elements by conodont apatite. *Palaeogeogr. Palaeoclim. Palaeoecol.* **2016**, *458*, 176–197. [[CrossRef](#)]
16. Dostal, J. Rare earth element deposits of alkaline igneous rocks. *Resources* **2017**, *6*, 34. [[CrossRef](#)]
17. Huang, J.; Tan, W.; Liang, X.; He, H.; Ma, L.; Bao, Z.; Zhu, J. REE fractionation controlled by REE speciation during formation of the Renju regolith-hosted REE deposits in Guangdong Province, South China. *Ore Geol. Rev.* **2021**, *134*, 104172. [[CrossRef](#)]
18. Chau, N.D.; Jadwiga, P.; Adam, P.; Van Hao, D.; Le Khanh Phon, J.P. General characteristics of rare earth and radioactive elements in Dong Pao deposit, Lai Chau, Vietnam. *Vietnam J. Earth Sci.* **2017**, *39*, 14–26. [[CrossRef](#)]
19. Fan, H.R.; Hu, F.F.; Yang, K.F.; Pirajno, F.; Liu, X.; Wang, K.Y. Integrated U–Pb and Sm–Nd geochronology for a REE-rich carbonatite dyke at the giant Bayan Obo REE deposit, Northern China. *Ore Geol. Rev.* **2014**, *63*, 510–519. [[CrossRef](#)]
20. Yang, X.J.; Lin, A.; Li, X.L.; Wu, Y.; Zhou, W.; Chen, Z. China’s ion-adsorption rare earth resources, mining consequences and preservation. *Environ. Dev.* **2013**, *8*, 131–136. [[CrossRef](#)]
21. Mastalerz, M.; Drobnik, A.; Eble, C.; Ames, P.; McLaughlin, P. Rare earth elements and yttrium in Pennsylvanian coals and shales in the eastern part of the Illinois Basin. *Int. J. Coal Geol.* **2020**, *231*, 103620. [[CrossRef](#)]
22. Seredin, V.V.; Dai, S. Coal deposits as potential alternative sources for lanthanides and yttrium. *Int. J. Coal Geol.* **2012**, *94*, 67–93. [[CrossRef](#)]
23. Moldoveanu, G.A.; Papangelakis, V.G. An overview of rare-earth recovery by ion-exchange leaching from ion-adsorption clays of various origins. *Miner. Mag.* **2016**, *80*, 63–76. [[CrossRef](#)]
24. Emsbo, P.; McLaughlin, P.L.; Breit, G.N.; du Bray, E.A.; Koenig, A.E. Rare earth elements in sedimentary phosphate deposits: Solution to the global REE crisis? *Gondwana Res.* **2015**, *27*, 776–785. [[CrossRef](#)]
25. Laurino, J.P.; Mustacato, J.; Huba, Z.J. Rare Earth Element Recovery from Acidic Extracts of Florida Phosphate Mining Materials Using Chelating Polymer 1-Octadecene, Polymer with 2,5-Furandione, Sodium Salt. *Minerals* **2019**, *9*, 477. [[CrossRef](#)]
26. Hower, J.C.; Granite, E.J.; Mayfield, D.B.; Lewis, A.S.; Finkelman, R.B. Notes on contributions to the science of rare earth element enrichment in coal and coal combustion by-products. *Minerals* **2016**, *6*, 32. [[CrossRef](#)]
27. Kolker, A.; Scott, C.; Hower, J.C.; Vazquez, J.A.; Lopano, C.L.; Dai, S. Distribution of rare earth elements in coal combustion fly ash determined by SHRIMP-RG ion microprobe. *Int. J. Coal Geol.* **2017**, *184*, 1–10. [[CrossRef](#)]
28. Dai, S.; Finkelman, R.B. Coal as a promising source of critical elements: Progress and future prospects. *Int. J. Coal Geol.* **2018**, *186*, 155–164. [[CrossRef](#)]
29. Seredin, V.V.; Dai, S.; Sun, Y.; Chekryzhov, I.Y. Coal deposits as promising sources of rare metals for alternative power and energy-efficient technologies. *Appl. Geochem.* **2013**, *31*, 1–11. [[CrossRef](#)]
30. Tourtelot, H.A. Black shale—Its deposition and diagenesis. *Clay Clay Miner.* **1979**, *27*, 313–321. [[CrossRef](#)]
31. Ripley, E.M.; Shaffer, N.R.; Gilstrap, M.S. Distribution and geochemical characteristics of metal enrichment in the New Albany Shale (Devonian-Mississippian), Indiana. *Econ. Geol.* **1990**, *85*, 1790–1807. [[CrossRef](#)]
32. Lev, S.M.; McLennan, S.; Meyers, W.J.; Hanson, G.N. A petrographic approach for evaluating trace-element mobility in a black shale. *J. Sediment. Res.* **1998**, *68*, 970–980. [[CrossRef](#)]
33. Lev, S.M.; McLennan, S.; Hanson, G.N. Mineralogical controls on REE mobility during black-shale diagenesis. *J. Sediment. Res.* **1999**, *69*, 1071–1082. [[CrossRef](#)]

34. Cruse, A.M.; Lyons, T.W.; Kidder, D.L. Rare-earth element behaviour in phosphate and organic-rich host shales. In *Marine Authigenesis: From Global to Microbial*; Glenn, C.R., Prévot-Lucas, L., Lucas, J., Eds.; SEPM Special Publications: Tulsa, OK, USA, 2000; Volume 66, pp. 445–453.
35. Brumsack, H.-J. The trace metal content of recent organic carbon-rich sediments: Implications for Cretaceous black shale formation. *Palaeogeogr. Palaeoclimatol. Palaeoecol.* **2006**, *232*, 344–361. [[CrossRef](#)]
36. Leybourne, M.I.; Johannesson, K.H. Rare earth elements (REE) and yttrium in stream waters, stream sediments, and Fe–Mn oxyhydroxides: Fractionation, speciation, and controls over REE + Y patterns in the surface environment. *Geochim. Cosmochim. Acta* **2008**, *72*, 5962–5983. [[CrossRef](#)]
37. Bai, J.-R.; Wang, Q.; Wei, Y.-Z.; Liu, T. Geochemical occurrences of rare earth elements in oil shale from Huadian. *J. Fuel Chem. Technol.* **2011**, *39*, 489–494. [[CrossRef](#)]
38. Fu, X.; Wang, J.; Zeng, Y.; Tan, F.; He, J. Geochemistry and origin of rare earth elements (REEs) in the Shengli River oil shale, northern Tibet, China. *Geochemistry* **2011**, *71*, 21–30. [[CrossRef](#)]
39. Pi, D.-H.; Liu, C.-Q.; Shields-Zhou, G.A.; Jiang, S.-Y. Trace and rare earth element geochemistry of black shale and kerogen in the early Cambrian Niutitang Formation in Guizhou province, South China: Constraints for redox environments and origin of metal enrichments. *Precambrian Res.* **2013**, *225*, 218–229. [[CrossRef](#)]
40. Yang, J.; Torres, M.; McManus, J.; Algeo, T.J.; Hakala, J.A.; Verba, C. Controls on rare earth element distributions in ancient organic-rich sedimentary sequences: Role of post-depositional diagenesis of phosphorus phases. *Chem. Geol.* **2017**, *466*, 533–544. [[CrossRef](#)]
41. Xu, J.; Cheng, B.; Deng, Q.; Liang, Y.; Faboya, O.L.; Liao, Z. Distribution and geochemical significance of trace elements in shale rocks and their residual kerogens. *Acta Geochim.* **2018**, *37*, 886–900. [[CrossRef](#)]
42. El-Anwar, E.A.A.; Abdelhafiz, M.A.; Salman, S.A. Rare earth and trace elements enrichment and implications in black shales of Safaga–Qussier sector, Egypt. *J. Afr. Earth Sci.* **2022**, *188*, 104482. [[CrossRef](#)]
43. Condie, K.C. Another look at rare earth elements in shales. *Geochim. Cosmochim. Acta* **1991**, *55*, 2527–2531. [[CrossRef](#)]
44. Phan, T.T.; Hakala, J.A.; Lopano, C.L.; Sharma, S. Rare earth elements and radiogenic strontium isotopes in carbonate minerals reveal diagenetic influence in shales and limestones in the Appalachian. *Basin. Chem. Geol.* **2019**, *509*, 194–212. [[CrossRef](#)]
45. Komarneni, S.; Roy, D.M. Hydrothermal Effects on Cesium Sorption and Fixation by Clay Minerals and Shales. *Clays Clay Miner.* **1980**, *28*, 142–149. [[CrossRef](#)]
46. Liu, C.; Zachara, J.M.; Qafoku, O.; Smith, S.C. Effect of temperature on Cs⁺ sorption and desorption in subsurface sediments at the Hanford Site, USA. *Environ. Sci. Technol.* **2003**, *37*, 2640–2645. [[CrossRef](#)]
47. Durrant, C.B.; Begg, J.D.; Kersting, A.B.; Zavarin, M. Cesium sorption reversibility and kinetics on illite, montmorillonite, and kaolinite. *Sci. Total Environ.* **2018**, *610–611*, 511–520. [[CrossRef](#)]
48. Palmer, C.A.; Lyons, P.C.; Brown, Z.A.; Mee, S.J. The use of rare earth and trace element concentrations in vitrinite concentrates and companion whole coals (hvA) bituminous to determine organic and inorganic associations. In *Recent Advances in Coal Geochemistry, Geological Society of America Special Paper*; Chyi, L.L., Chou, C.-L., Eds.; Geological Society of America: Boulder, CO, USA, 1990; Volume 248, pp. 55–62.
49. Elderfield, H.; Upstill-Goddard, R.; Sholkovitz, E.R. The rare earth elements in rivers, estuaries, and coastal seas and their significance to the composition of ocean waters. *Geochim. Cosmochim. Acta* **1990**, *54*, 971–991. [[CrossRef](#)]
50. Hower, J.C.; Ruppert, L.F.; Eble, C.F. Lanthanide, yttrium, and zirconium anomalies in the Fire Clay coal bed, Eastern Kentucky. *Int. J. Coal Geol.* **1999**, *39*, 141–153. [[CrossRef](#)]
51. Seredin, V.V. Rare earth element-bearing coals from the Russian Far East deposits. *Int. J. Coal Geol.* **1996**, *30*, 101–129. [[CrossRef](#)]
52. Seredin, V.V.; Finkelman, R.B. Metalliferous coals: A review of the main genetic and geochemical types. *Int. J. Coal Geol.* **2008**, *76*, 253–289. [[CrossRef](#)]
53. Henderson, P. The rare earth elements: Introduction and review. In *Rare Earth Minerals: Chemistry, Origin and Ore Deposits*; Chapman and Hall: London, UK, 1996; pp. 1–19.
54. Leybourne, M.I.; Goodfellow, W.D.; Boyle, D.R.; Hall, G.M. Rapid development of negative Ce anomalies in surface waters and contrasting REE patterns in groundwaters associated with Zn–Pb massive sulphide deposits. *Appl. Geochem.* **2000**, *15*, 695–723. [[CrossRef](#)]
55. Bau, M.; Dulski, P. Comparing yttrium and rare earths in hydrothermal fluids from the Mid-Atlantic Ridge: Implications for Y and REE behaviour during near-vent mixing and for the Y/Ho ratio of Proterozoic seawater. *Chem. Geol.* **1999**, *155*, 77–90. [[CrossRef](#)]
56. Ver Straeten, C.A.; Tollo, R.P.; Bartholomew, M.J.; Hibbard, J.P.; Karabinos, P.M. Lessons from the foreland basin: Northern Appalachian basin perspectives on the Acadian orogeny. In *From Rodinia to Pangea: The Lithotectonic Record of the Appalachian Region*; Geological Society of America: Boulder, CO, USA, 2010; Volume 206, pp. 251–282.
57. Etensohn, F.R. Compressional tectonic controls on epicontinental black-shale deposition: Devonian–Mississippian examples from North America. In *Shales and Mudstones; Basin Studies, Sedimentology, and Paleontology*; E. Schweizerbart'sche Verlagsbuchhandlung: Stuttgart, Germany, 1998; Volume I, pp. 109–128.
58. Martin, J.P. The Middle Devonian Hamilton group shales in the northern Appalachian basin: Production and potential. In *American Association of Petroleum Geologists Eastern Section Abstracts*; American Association of Petroleum Geologists: Buffalo, NY, USA, 2006.

59. Hammes, U.; Hamlin, H.S.; Ewing, T.E. Geologic analysis of the Upper Jurassic Haynesville Shale in east Texas and west Louisiana. *AAPG Bull.* **2011**, *95*, 1643–1666. [[CrossRef](#)]
60. Ewing, T.E. Review of Late Jurassic depositional systems and potential hydrocarbon plays, northern Gulf of Mexico Basin. *Gulf Coast Assoc. Geol. Soc. Trans.* **2001**, *51*, 85–96.
61. Spain, D.R.; Anderson, G.A. Controls on reservoir quality and productivity in the Haynesville Shale, northwestern Gulf of Mexico Basin. *Gulf Coast Assoc. Geol. Soc. Trans.* **2010**, *60*, 657–668.
62. Agrawal, V.; Sharma, S. Testing Utility of Organogeochemical Proxies to Assess Sources of Organic Matter, Paleoredox Conditions, and Thermal Maturity in Mature Marcellus Shale. *Front. Energy Res.* **2018**, *6*, 42. [[CrossRef](#)]
63. Tessier, A.P.G.C.; Campbell, P.G.; Bisson, M.J.A.C. Sequential extraction procedure for the speciation of particulate trace metals. *Anal. Chem.* **1979**, *51*, 844–851. [[CrossRef](#)]
64. Riley, K.W.; French, D.H.; Farrell, O.P.; Wood, R.A.; Huggins, F.E. Modes of occurrence of trace and minor elements in some Australian coals. *Int. J. Coal Geol.* **2012**, *94*, 214–224. [[CrossRef](#)]
65. Available online: <https://www.epa.gov/esam/method-2007-determination-metals-and-trace-elements-water-and-wastes-in-ductively-coupled-plasma> (accessed on 20 May 2021).
66. Available online: <https://www.usgs.gov/media/files/60-elements-icp-oes-ms-na2o-fusion-method> (accessed on 20 May 2021).
67. Pilewski, J.; Sharma, S.; Agrawal, V.; Hakala, J.A.; Stuckman, M.Y. Effect of maturity and mineralogy on fluid-rock reactions in the Marcellus Shale. *Environ. Sci. Process. Impacts* **2019**, *21*, 845–855. [[CrossRef](#)]
68. Bright, C.A.; Cruse, A.M.; Lyons, T.W.; MacLeod, K.G.; Glascock, M.D.; Ethington, R.L. Seawater rare-earth element patterns preserved in apatite of Pennsylvanian conodonts? *Geochim. Cosmochim. Acta* **2009**, *73*, 1609–1624. [[CrossRef](#)]
69. Byrne, R.H.; Kim, K.-H. Rare earth precipitation and coprecipitation behavior: The limiting role of PO₄³⁻ on dissolved rare earth concentrations in seawater. *Geochim. Cosmochim. Acta* **1993**, *57*, 519–526. [[CrossRef](#)]
70. Byrne, R.H.; Liu, X.; Schijf, J. The influence of phosphate coprecipitation on rare earth distributions in natural waters. *Geochim. Cosmochim. Acta* **1996**, *60*, 3341–3346. [[CrossRef](#)]
71. Elderfield, H.; Greaves, M.J. The rare earth elements in seawater. *Nature* **1982**, *296*, 214–219. [[CrossRef](#)]
72. Sholkovitz, E.R.; Landing, W.M.; Lewis, B.L. Ocean particle chemistry: The fractionation of rare earth elements between suspended particles and seawater. *Geochim. Cosmochim. Acta* **1994**, *58*, 1567–1579. [[CrossRef](#)]
73. Kim, T.H.; Waska, H.; Kwon, E.; Suryaputra, I.G.N.; Kim, G. Production, degradation, and flux of dissolved organic matter in the subterranean estuary of a large tidal flat. *Mar. Chem.* **2012**, *142*, 1–10. [[CrossRef](#)]
74. Cantrell, K.J.; Byrne, R.H. Rare earth element complexation by carbonate and oxalate ions. *Geochim. Cosmochim. Acta* **1987**, *51*, 597–605. [[CrossRef](#)]
75. Pourret, O.; Davranche, M.; Gruau, G.; Dia, A. Competition between humic acid and carbonates for rare earth elements complexation. *J. Colloid Interface Sci.* **2007**, *305*, 25–31. [[CrossRef](#)]
76. Pourret, O.; Davranche, M.; Gruau, G.; Dia, A. New insights into cerium anomalies in organic-rich alkaline waters. *Chem. Geol.* **2008**, *251*, 120–127. [[CrossRef](#)]
77. Jarvis, I.; Burnett, W.C.; Nathan, Y.; Almbaydin, F.S.M.; Attia, A.K.M.; Castro, L.N.; Flicoteaux, R.; Hilmy, M.E.; Husain, V.; Qutawnah, A.A.; et al. Phosphorite geochemistry—State-of-the-art and environmental concerns. *Eclogae Geol. Helv. J. Swiss Geol. Soc.* **1994**, *87*, 643–700.
78. Lefticariu, L.; Klitzing, K.L.; Kolker, A. Rare Earth Elements and Yttrium (REY) in coal mine drainage from the Illinois Basin, USA. *Int. J. Coal Geol.* **2020**, *217*, 103327. [[CrossRef](#)]
79. Coveney, R.M., Jr.; Leventhal, J.S.; Glascock, M.D.; Hatch, J. Origins of metals and organic matter in the Mecca Quarry Shale Member and stratigraphically equivalent beds across the Midwest. *Econ. Geol.* **1987**, *82*, 915–933. [[CrossRef](#)]
80. Finkelman, R.B.; Dai, S.; French, D. The importance of minerals in coal as the hosts of chemical elements: A review. *Int. J. Coal Geol.* **2019**, *212*, 103251. [[CrossRef](#)]
81. Li, L.Z.; Yang, X. China's rare earth resources, mineralogy, and beneficiation. In *Rare Earths Industry*; Elsevier: Amsterdam, The Netherlands, 2016; pp. 139–150.
82. Chen, R.; Sharma, S. Linking the Acadian Orogeny with organic-rich black shale deposition: Evidence from the Marcellus Shale. *Mar. Pet. Geol.* **2017**, *79*, 149–158. [[CrossRef](#)]
83. Chen, R.; Sharma, S. Role of alternating redox conditions in the formation of organic-rich interval in the Middle Devonian Marcellus Shale, Appalachian Basin, USA. *Palaeogeogr. Palaeoclim. Palaeoecol.* **2016**, *446*, 85–97. [[CrossRef](#)]
84. Ver Straeten, C.A. The classic Devonian of the Catskill Front: A foreland basin record of Acadian orogenesis. In Proceedings of the New York State Geological Association Field Trip Guidebook 81st Annual Meeting, New York, NY, USA, 25–27 September 2009; pp. 7-1–7-54.
85. Murphy, J.B.; Van Staal, C.R.; Keppie, J.D. Middle to late Paleozoic Acadian orogeny in the northern Appalachians: A Laramide-style plume-modified orogeny? *Geology* **1999**, *27*, 653–656. [[CrossRef](#)]
86. Agrawal, V.; Sharma, S. Molecular characterization of kerogen and its implications for determining hydrocarbon potential, organic matter sources and thermal maturity in Marcellus Shale. *Fuel* **2018**, *228*, 429–437. [[CrossRef](#)]
87. Agrawal, V.; Sharma, S. Are we modeling the properties of unconventional shales correctly? *Fuel* **2020**, *267*, 117316. [[CrossRef](#)]
88. Bayon, G.; German, C.R.; Burton, K.W.; Nesbitt, R.W.; Rogers, N. Sedimentary Fe–Mn oxyhydroxides as paleoceanographic archives and the role of aeolian flux in regulating oceanic dissolved REE. *Earth Planet. Sci. Lett.* **2004**, *224*, 477–492. [[CrossRef](#)]

89. Gutjahr, M.; Frank, M.; Stirling, C.H.; Klemm, V.; Van de Fliedrt, T.; Halliday, A.N. Reliable extraction of a deepwater trace metal isotope signal from Fe–Mn oxyhydroxide coatings of marine sediments. *Chem. Geol.* **2007**, *242*, 351–370. [[CrossRef](#)]
90. Haley, B.A.; Frank, M.; Hathorne, E.; Piasias, N. Biogeochemical implications from dissolved rare earth element and Nd isotope distributions in the Gulf of Alaska. *Geochim. Et Cosmochim. Acta* **2014**, *126*, 455–474. [[CrossRef](#)]
91. Tostevina, R.; Shieldsa, G.A.; Tarbucka, G.M.; He, T.; Clarkson, M.O.; Wood, R.A. Effective use of cerium anomalies as a redox proxy in carbonate-dominated marine settings. *Chem. Geol.* **2016**, *438*, 146–162. [[CrossRef](#)]
92. Freslon, N.; Bayon, G.; Toucanne, S.; Bermell, S.; Bollinger, C.; Chéron, S.; Etoubleau, J.; Germain, Y.; Khripounoff, A.; Ponzevera, E.; et al. Rare earth elements and neodymium isotopes in sedimentary organic matter. *Geochim. Cosmochim. Acta* **2014**, *140*, 177–198. [[CrossRef](#)]
93. Blood, D.R.; Lash, G.G.; Larsen, D.; Egenhoff, S.O.; Fishman, N.S. Dynamic redox conditions in the Marcellus Shale as recorded by pyrite framboid size distributions. *Geol. Soc. Am. Spec. Pap.* **2015**, *515*, 153–168.
94. Lash, G.G.; Blood, D.R. Organic matter accumulation, redox, and diagenetic history of the Marcellus Formation, southwestern Pennsylvania, Appalachian basin. *Mar. Pet. Geol.* **2014**, *57*, 244–263. [[CrossRef](#)]
95. Phan, T.T.; Gardiner, J.B.; Capo, R.C.; Stewart, B.W. Geochemical and multiisotopic ($^{87}\text{Sr}/^{86}\text{Sr}$, $^{143}\text{Nd}/^{144}\text{Nd}$, $^{238}\text{U}/^{235}\text{U}$) perspectives of sediment sources, depositional conditions, and diagenesis of the Marcellus Shale. *Appalach. Basin* **2018**, *222*, 187–211.
96. Sageman, B.B.; Murphy, A.E.; Werne, J.P.; Ver Straeten, C.A.; Hollander, D.J.; Lyons, T.W. A tale of shales: The relative roles of production, decomposition, and dilution in the accumulation of organic-rich strata, Middle–Upper Devonian, Appalachian basin. *Chem. Geol.* **2003**, *195*, 229–273. [[CrossRef](#)]
97. Werne, J.P.; Sageman, B.B.; Lyons, T.W.; Hollander, D.J. An integrated assessment of a “type euxinic” deposit: Evidence for multiple controls on black shale deposition in the Middle Devonian Oatka Creek Formation. *Am. J. Sci.* **2002**, *302*, 110–143. [[CrossRef](#)]
98. Kidder, D.L.; Krishnaswamy, R.; Mapes, R.H. Elemental mobility in phosphatic shales during concretion growth and implications for provenance analysis. *Chem. Geol.* **2003**, *198*, 335–353. [[CrossRef](#)]
99. Haley, B.A.; Klinkhammer, G.P.; McManus, J. Rare earth elements in pore waters of marine sediments. *Geochim. Cosmochim. Acta* **2004**, *68*, 1265–1279. [[CrossRef](#)]
100. Ruttenberg, K.C. Development of a sequential extraction method for different forms of phosphorus in marine sediments. *Limnology and oceanography* **1992**, *37*, 1460–1482. [[CrossRef](#)]
101. Anderson, L.D.; Delaney, M.L. Sequential extraction and analysis of phosphorus in marine sediments: Streamlining of the SEDEX procedure. *Limnol. Oceanogr.* **2000**, *45*, 509–515. [[CrossRef](#)]
102. Wu, Y.; Mirza, N.R.; Hu, G.; Smith, K.H.; Stevens, G.W.; Mumford, K.A. Precipitating characteristics of potassium bicarbonate using concentrated potassium carbonate solvent for carbon dioxide capture. Part 1. Nucleation. *Ind. Eng. Chem. Res.* **2017**, *56*, 6764–6774. [[CrossRef](#)]
103. Mihajlovic, J.; Rinklebe, J. Rare earth elements in German soils—A review. *Chemosphere* **2018**, *205*, 514–523. [[CrossRef](#)]
104. Donmoyer, S.; Agrawal, V.; Sharma, S.; Hakala, J.A. Effect of Oxidative Breakers on Organic Matter Degradation, Contaminant Mobility and Critical Mineral Release during Shale-Fracturing Fluid Interactions in the Marcellus Shale. *Fuel* **2023**, *331*, 125678. [[CrossRef](#)]
105. Ferguson, B.; Agrawal, V.; Sharma, S.; Hakala, J.A.; Xiong, W. Effects of Carbonate Minerals on Shale-Hydraulic Fracturing Fluid Interactions in the Marcellus Shale. *Front. Earth Sci.* **2021**, *9*, 1072. [[CrossRef](#)]
106. Gao, Y.; Liang, K.; Gou, Y.; Wei, S.; Shen, W.; Cheng, F. Aluminum extraction technologies from high aluminum fly ash. *Rev. Chem. Eng.* **2021**, *37*, 885–906. [[CrossRef](#)]
107. Zhang, R.; Zhang, C.; Cao, Y. The enhanced extraction of rare earth elements from coal gangue and coal fly ash. *Res. Sq.* **2022**. [[CrossRef](#)]
108. Tian, L.; Chang, H.; Tang, P.; Li, T.; Zhang, X.; Liu, S.; He, Q.; Wang, T.; Yang, J.; Bai, Y.; et al. Rare earth elements occurrence and economical recovery strategy from shale gas wastewater in the Sichuan Basin, China. *ACS Sustain. Chem. Eng.* **2020**, *8*, 11914–11920. [[CrossRef](#)]
109. Seredin, V.V. A new method for primary evaluation of the outlook for rare earth element ores. *Geol. Ore Depos.* **2010**, *52*, 428–433. [[CrossRef](#)]